SIMPLE AND EFFICIENT HIGH-PERFORMANCE PWM ALGORITHM FOR INDUCTION MOTOR DRIVES

P. RAMA MOHAN
Associate Professor, E.E.E Department, Krishna's Pragati Institute of Technology, Rajahmundry, A.P, India,
rammohan_cdp@yahoo.co.in

T. BRAMHANANDA REDDY
Professor, E.E.E Department, G. Pulla Reddy Engineering College, Kurnool, Andhra Pradesh, India
tbnr@rediffmail.com

M. VIJAYA KUMAR
Professor, E.E.E Department, J.N.T. University, Anantapur, Andhra Pradesh, India
mvk_2004@rediffmail.com

Abstract: *This paper presents a simple generalized pulse width modulation algorithm for induction motor drives. The conventional space vector approach requires the angle and sector information to calculate the actual gating times of the inverter, which increases the complexity of the pulsewidth modulation algorithm. Hence to reduce the complexity, the proposed approach generates the actual gating times from the instantaneous sampled reference phase voltages only. Moreover, the proposed generalized pulse width modulation algorithm uses a unified expression for offset time from which by varying a parameter various PWM algorithms cam be generated. The current ripple characteristics of various pulsewidth modulation algorithms are analytically modelled. With the aid of these characteristics, high performance pulsewidth modulation algorithm has been developed. To verify the proposed high performance pulsewidth modulation algorithm, numerical simulation studies have been carried out and results have been presented.*

Key words: *current ripple, generalized pulsewidth modulation, high-performance pulsewidth modulation, induction motor drive, space vector pulsewidth modulation*

1. Introduction

Nowadays the voltage source inverters (VSI) are becoming popular in many industrial drive applications. The variable speed drive applications require variable voltage, variable frequency voltages, which can be obtained from a VSI. At present, there are many voltage modulation methods for VSI in order to obtain variable voltage and variable frequency supply voltages. A detailed survey on various pulse width modulation (PWM) algorithms is given in [1]. Of the various PWM algorithms, space vector PWM (SVPWM) is popular due to its numerous advantages when compared with the sinusoidal PWM (SPWM) algorithm [2]. The SVPWM algorithm distributes the zero voltage vector time equally among the two possible zero voltage vectors. The SVPWM algorithm gives superior performance at lower modulation indices. Moreover, as the SVPWM algorithm is a continuous PWM (CPWM) algorithm it gives more switching losses of the inverter. By utilizing the freedom of division of zero state time, various discontinuous PWM (DPWM) algorithms can be generated. The DPWM methods result in reduced switching losses and reduced harmonic distortion at higher modulation indices [3-7]. To analyze the PWM algorithms in view of harmonic distortion, expressions have been derived in a simple form by using the notion of stator flux ripple in [3]. Also, by using the notion of current ripple, expressions for harmonic distortion have been derived in [7-8]. However, the conventional space vector approach [2-8] requires the angle and sector information for the calculation of gating signals, which increases the complexity involved in the PWM algorithm. To reduce the complexity involved in the conventional space vector approach, a unified voltage modulation algorithm have been developed in [9] by using the concept effective time.

This paper presents a generalized PWM (GPWM) algorithm, which uses an unified offset time expression. By varying zero voltage vector time partition factor (k_o) in the proposed PWM algorithm various DPWM algorithms can be generated along with the SVPWM algorithm. Moreover, the current ripple analysis of various PWM algorithms has been presented from which high performance PWM algorithm has been developed.

2. Proposed GPWM algorithm

As the conventional space vector approach requires the angle and sector information, the complexity involved in the PWM algorithm is more. Hence, to reduce the complexity involved in the conventional space vector approach, the proposed GPWM algorithm uses the notion of imaginary switching times. Assume the three-phase reference phase voltages as given in (1) and (2).

$$V_{in} = V_{ref}\ cos\left(\theta - 2(r-1)\pi/3\right) \quad (1)$$

$$V_{ix} = V_{ref}\ cos\left(\theta - 2(r-1)\pi/3 - \pi/6\right) \quad (2)$$

where i =a, b, c and r =1, 2, 3. The values of

imaginary switching times are directly proportional to the instantaneous phase voltages and can be defined as in (3) and (4) [9-10].

$$T_{in} = \frac{V_{in}}{V_{dc}} T_s \qquad i = a,b,c \tag{3}$$

$$T_{ix} = \frac{V_{ix}}{V_{dc}} T_s \qquad i = a,b,c \tag{4}$$

These switching times may be negative when the corresponding phase voltage is negative and hence these are called as imaginary switching times. The maximum, medium and minimum imaginary switching times can be evaluated in each sampling time period from (5).

$$T_{\max} = \max(T_{in}); T_{mid} = mid(T_{in}); T_{\min} = \min(T_{in}) \tag{5}$$

$$T_{\max,x} = \max(T_{ix}); T_{mid,x} = mid(T_{ix}); T_{\min,x} = \min(T_{ix}) \tag{6}$$

Then, the actual switching times of the active states can be calculated as given in (7) [10].

$$T_k = T_{\max} - T_{mid}; \; T_{k+1} = T_{mid} - T_{\min} \tag{7}$$

The zero voltage vector time can be calculated as given in (8).

$$T_z = T_s - T_k - T_{k+1} = T_s - T_{\max} + T_{\min} \tag{8}$$

To generate the various DPWM algorithms along with the SVPWM algorithm, the proposed algorithm utilizes the unequal distribution of zero state time. The proposed algorithm divides the zero state time among the two possible zero voltage vectors as given in (9).

$$T_0 = k_o T_z; T_7 = (1 - k_o) T_z \tag{9}$$

Then the generalized expressions for the actual gating times in terms of the unified offset time are as given in (10).

$$T_{gi} = T_{in} + T_{offset} \tag{10}$$

where $T_{offset} = T_s(1 - k_o) + (k_o - 1)T_{\max} - k_o T_{\min}$.

In the proposed GPWM algorithm, by varying the zero voltage vector time partition parameter (k_o) between 0 and 1, various PWM algorithms can be generated as shown in Table.1

Table 1: Generation of various PWM algorithms by varying k_o value

PWM algorithm	k_o value
SVPWM	0.5
DPWMMIN	1
DPWMMAX	0
DPWM0	*if* $T_{\max,x} + T_{\min,x} < 0 \Rightarrow k_o = 0$ *if* $T_{\max,x} + T_{\min,x} \geq 0 \Rightarrow k_o = 1$
DPWM1	*if* $T_{\max} + T_{\min,} < 0 \Rightarrow k_o = 1$ *if* $T_{\max} + T_{\min} \geq 0 \Rightarrow k_o = 0$
DPWM2	*if* $T_{\max,x} + T_{\min,x} < 0 \Rightarrow k_o = 1$ *if* $T_{\max,x} + T_{\min,x} \geq 0 \Rightarrow k_o = 0$
DPWM3	*if* $T_{\max} + T_{\min,} < 0 \Rightarrow k_o = 0$ *if* $T_{\max} + T_{\min} \geq 0 \Rightarrow k_o = 1$

The modulation index (M_i) can be defined as "the ratio of the required peak fundamental magnitude to the maximum fundamental output in six-step mode" and given in (11).

$$M_i = \frac{|V_{ref}|}{V_{\max,sixstep}} = \frac{\pi V_{ref}}{2V_{dc}} \tag{11}$$

The modulating waveforms of various PWM algorithms at different modulation indices are as shown in Fig. 1-Fig.7.

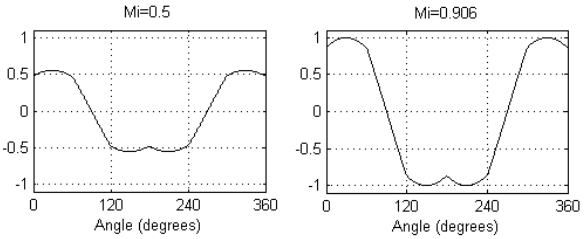

Fig. 1 modulating waveforms for SVPWM

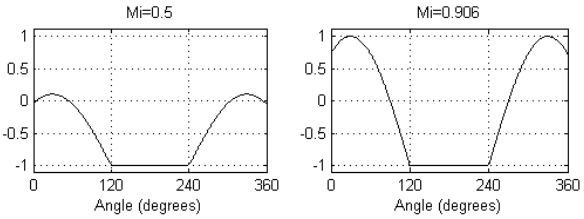

Fig. 2 modulating waveforms for DPWMMIN

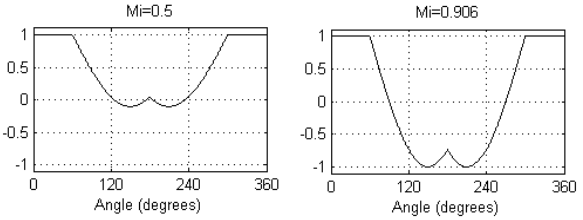

Fig. 3 modulating waveforms for DPWMMAX

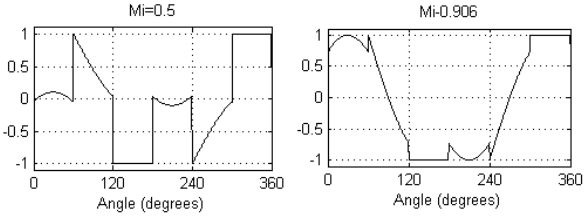

Fig. 4 modulating waveforms for DPWM0

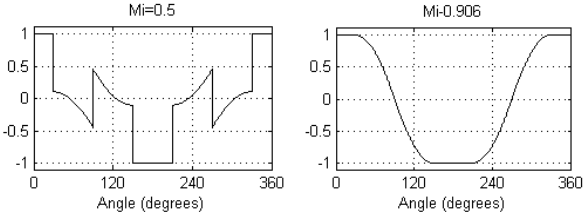

Fig. 5 modulating waveforms for DPWM1

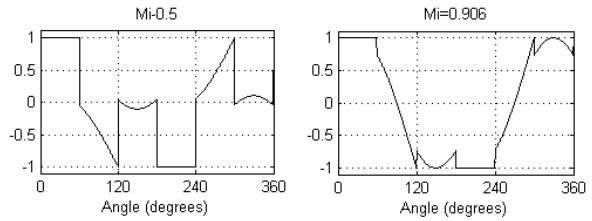

Fig. 6 modulating waveforms for DPWM2

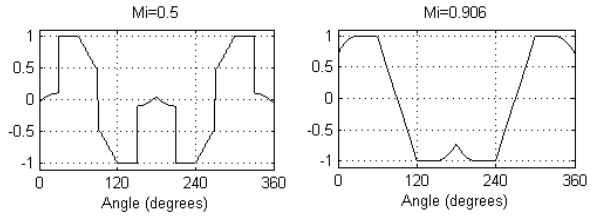

Fig. 7 modulating waveforms for DPWM3

3. RMS Current Ripple Analysis

In the space vector approach, the reference voltage vector will be constructed in the average manner over a sampling time period but not in instantaneous fashion. Hence, there is always a ripple voltage vector between the applied and reference voltage vectors. The error voltage vector can be defined as given in (12)

$$V_{rip} = V_{applied} - V_{ref} \tag{12}$$

The allied voltage vector may be any one of the possible voltage vectors (from V_0 to V_7). From the voltage ripple vector, the current ripple vector can be calculated by using (13).

$$i_{rip} = \frac{1}{\sigma L_s}\int_0^t V_{rip}\,dt \tag{13}$$

The proposed GPWM algorithm uses 0127-7210 sequence when $k_o = 0.5$, 012-210 sequence when $k_o = 1$ and 721-127 sequence when $k_o = 0$. The pole voltage waveforms along with the time interval of the proposed GPWM algorithm are as shown in Fig. 8 in the first sector. As the all sectors are symmetric, the analysis of current ripple is limited to the first sector only.

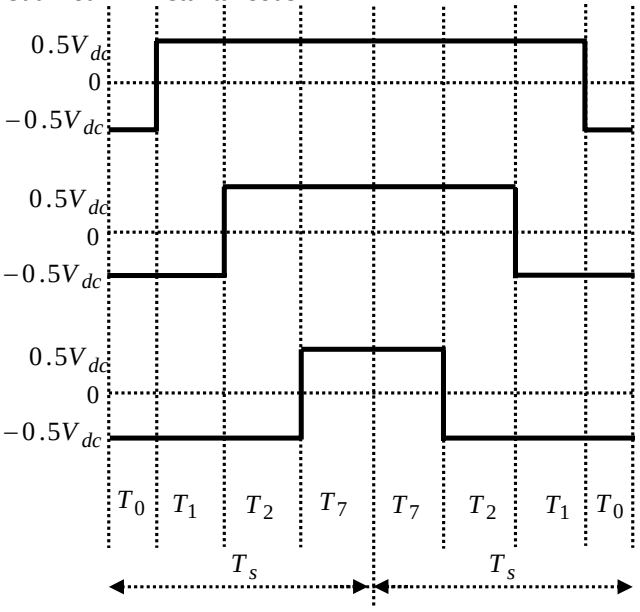

Fig. 8 the pole voltages for the proposed GPWM algorithms in the first sector

In the first sector, the voltage ripple vectors and the variation of the current ripple by the application of corresponding voltage vectors are shown in Fig. 9. Also, from this figure, it can be observed that the current ripple has zero mean value in a sampling time period. Then the current ripple vectors are given by as follows:

$$i_{r1} = \frac{V_1 - V_{ref}}{\sigma L_s}T_1 = \frac{V_{r1}}{\sigma L_s}T_1 \tag{14}$$

$$i_{r2} = \frac{V_2 - V_{ref}}{\sigma L_s}T_2 = \frac{V_{r2}}{\sigma L_s}T_2 \tag{15}$$

$$i_{rz} = -\frac{V_{ref}}{\sigma L_s}T_z = \frac{V_{rz}}{\sigma L_s}T_z \tag{16}$$

From Fig. 9, the d,q components of the voltage ripple vectors can be obtained as given in (17) – (19).

$$V_{r1d} = \frac{2}{3}V_{dc}\sin\alpha \;;\; V_{r1q} = \frac{2}{3}V_{dc}\cos\alpha - V_{ref} \tag{17}$$

$$V_{r2d} = -\frac{2}{3}V_{dc}\sin\left(60^o - \alpha\right);\; V_{r2q} = \frac{2}{3}V_{dc}\cos\left(60^o - \alpha\right) - V_{ref} \tag{18}$$

$$V_{rzd} = 0 \;;\; V_{rzq} = -V_{ref} \tag{19}$$

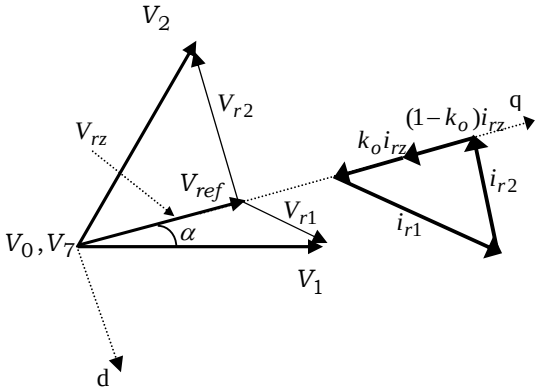

Fig. 9 Voltage ripple vectors and the corresponding current ripple vectors

The corresponding current ripple vectors can be given as below:

$$i_{r1} = i_{d1} + ji_{q1}$$

$$= \frac{\frac{2}{3}V_{dc}\sin\alpha}{\sigma L_s}T_1 + j\frac{\frac{2}{3}V_{dc}\cos\alpha - V_{ref}}{\sigma L_s}T_1 \quad (20)$$

$$i_{r2} = i_{d2} + ji_{q2}$$

$$= \frac{\frac{2}{3}V_{dc}\sin(60^o-\alpha)}{\sigma L_s}T_2 + j\frac{\frac{2}{3}V_{dc}\cos(60^o-\alpha) - V_{ref}}{\sigma L_s}T_2$$

$$= \frac{\frac{2}{3}V_{dc}\sin\alpha}{\sigma L_s}T_1 + j\frac{\frac{2}{3}V_{dc}\cos(60^o-\alpha) - V_{ref}}{\sigma L_s}T_2 \quad (21)$$

$$i_{rz} = i_{dz} + ji_{qz} = 0 + j\frac{-V_{ref}}{\sigma L_s}T_z \quad (22)$$

In the conventional space vector approach, the active voltage vector switching time expressions can be obtained as given in (23) and (24).

$$T_1 = \frac{2\sqrt{3}}{\pi}M_i\left(\sin(60^o-\alpha)\right)T_s \quad (23)$$

$$T_2 = \frac{2\sqrt{3}}{\pi}M_i\left(\sin\alpha\right)T_s \quad (24)$$

From (23) and (24) the expressions of $\sin\alpha$, $\cos\alpha$ and $\cos(60^o-\alpha)$ can be obtained as

$$\sin\alpha = \frac{\pi T_2}{2\sqrt{3}M_i T_s} \quad (25)$$

$$\cos\alpha = \frac{\pi(T_1 + 0.5T_2)}{3M_i T_s} \quad (26)$$

$$\cos(60^\circ-\alpha) = \frac{\pi(0.5T_1 + T_2)}{3M_i T_s} \quad (27)$$

By substituting (25), (26) and (27) in (20), (21) and (22), the d-axis and q-axis ripple expressions can be obtained as given in (28) – (30).

$$i_d = i_{d1} = i_{d2}\frac{T_1}{\sigma L_s}\left(\frac{\pi V_{dc}}{3\sqrt{3}M_i}\frac{T_2}{T_s}\right) \quad (28)$$

$$i_{q1} = \frac{T_1}{\sigma L_s}\left(\frac{2V_{dc}\pi(T_1 + 0.5T_2)}{9M_i T_s} - \frac{2V_{dc}M_i}{\pi}\right) \quad (29)$$

$$i_{q2} = \frac{T_2}{\sigma L_s}\left(\frac{2V_{dc}\pi(0.5T_1 + T_2)}{9M_i T_s} - \frac{2V_{dc}M_i}{\pi}\right) \quad (30)$$

The current ripple vectors shown in Fig. 9 can be resolved along d-and q-axis, which are fixed to the synchronously rotating reference frame as shown in Fig. 10.

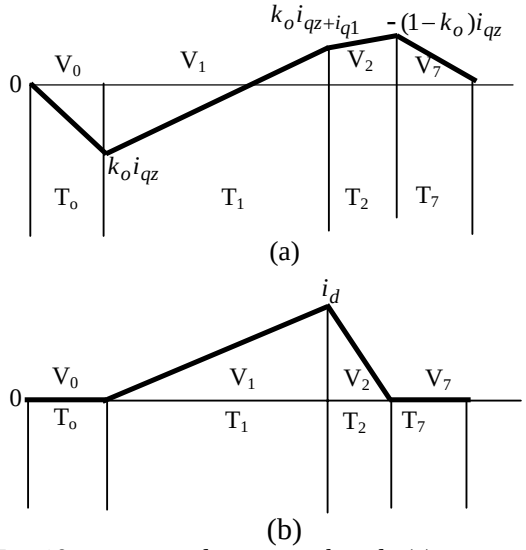

Fig. 10 current ripple over a subcycle (a) q-axis ripple (b) d-axis ripple

The q-axis, d-axis rms current ripple over a sampling time period or subcycle (T_s) can be given as in (31) and (32).

$$i^2_{q,rms,sub} = \frac{1}{T_s}\int_0^{T_s} i^2_{q,rip}\,dt \quad (31)$$

$$i^2_{d,rms,sub} = \frac{1}{T_s}\int_0^{T_s} i^2_{d,rip}\,dt \quad (32)$$

The total rms current ripple over a subcycle can be calculated using (33).

$$i^2_{rms,subcycle} = i^2_{q,rms,sub} + i^2_{d,rms,sub} \quad (33)$$

In the space vector approach, all the sectors are symmetrical and hence the integration of the square of the rms current ripple per subcycle over one sector gives the square of the rms current ripple as shown in (34)

$$i^2_{rms} = \frac{3}{\pi}\int_0^{\pi/3} i^2_{rms,subcycle}\;\;d\alpha \quad (34)$$

From Fig. 10, the expressions for q-axis and d-axis current ripple over a subcycle can be given as in (35) and (36).

$$i_{q,rms,sub}^2 = \frac{1}{3T_s}\left\{\begin{array}{l} k_o i_{qz})^2 T_o + \left((k_o i_{qz})^2 + (i_{q1} + k_o i_{qz})^2 + k_o i_{qz}(i_{q1} + k_o i_{qz})\right)T_1 \\ \left((i_{q1} + k_o i_{qz})^2 - (1-k_o) i_{qz}(i_{q1} + k_o i_{qz}) + ((1-k_o) i_{qz})^2\right)T_2 + \left((1-k_o) i_{qz})^2\right)T_7 \end{array}\right\} \quad (35)$$

$$i_{d,rms,sub}^2 = \frac{1}{3T_s} i_d^2 (T_1 + T_2) \quad (36)$$

The number of switchings of the SVPWM algorithm in a subcycle is three, whereas for the DPWM algorithms is two. Moreover, the DPWM algorithms clamp any one of the phases to either positive dc bus or negative dc bus for a total period of 120° over a fundamental cycle. Hence, the switching losses of the associated inverter leg are eliminated. Hence, the switching frequency of the above DPWM algorithms is reduced by 1/3 when compared with SVPWM algorithm. Hence a switching frequency coefficient can be introduced as defined in (37).

$$k_{sw} = \frac{f_{swCSVPWM}}{f_{swDPWM}} \quad (37)$$

To maintain constant average switching frequency, k_{sw} is taken as 2/3. Thus the proposed harmonic analysis is capable of estimating d-axis and q-axis stator current ripples individually. Total harmonic distortion (THD) of the current waveform is equally affected by the d-axis and q-axis current ripples. On the other hand, torque pulsation mainly depends on q-axis ripple, and is practically independent of d-axis current ripple. By using (33), the rms current ripple over a subcycle is plotted against the angle α with different modulation indices in Fig. 11 – Fig. 14.

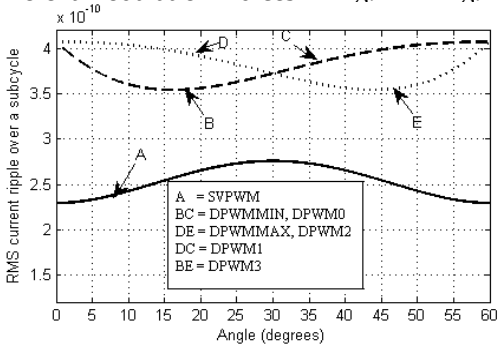

Fig. 11 RMS current ripple over a subcycle against the angle α at M_i=0.4.

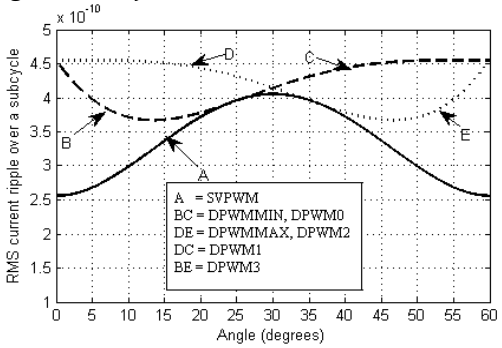

Fig. 12 RMS current ripple over a subcycle against the angle α at M_i=0.55.

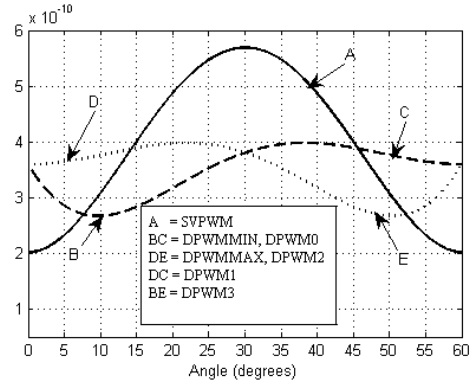

Fig. 13 RMS current ripple over a subcycle against the angle α at M_i=0.7.

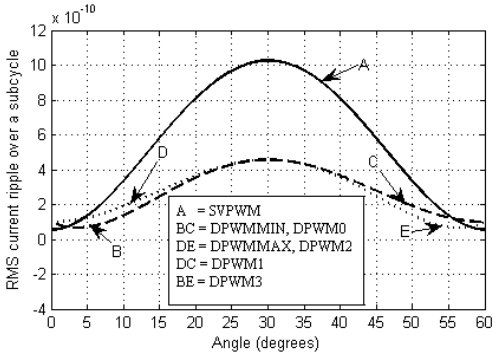

Fig. 14 RMS current ripple over a subcycle against the angle α at M_i=0.906.

The variation of RMS current ripple over a sixty degrees period (sector) against the modulation index is plotted as shown in Fig. 15.

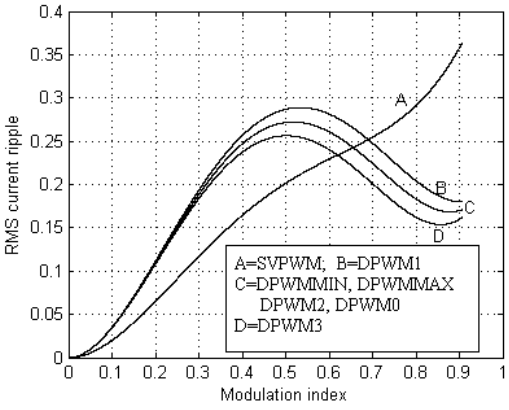

Fig. 15 RMS current ripple over a sixty degrees (sector) against the modulation index.

From (33), it can be observed that the RMS current ripple is a function of modulation index also. By comparing the RMS ripple characteristics of different PWM algorithms, the zones of superior performance can be obtained. A comparison of SVPWM algorithm with the other DPWM algorithms is presented in Fig. 16 – Fig. 19. These figures give the boundary between the regions of superior performance of SVPWM and other DPWM algorithms. SVPWM algorithm gives better performance below the boundary line and above the boundary line DPWM algorithms give better performance.

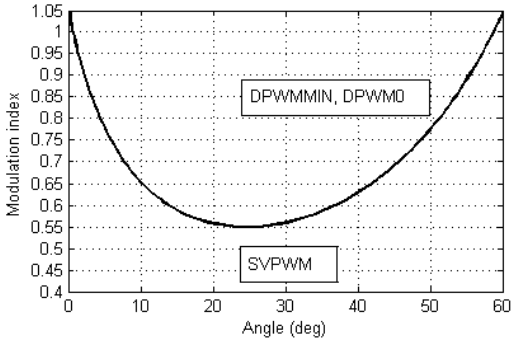

Fig. 16 boundary between SVPWM and DPWMMIN and DPWM0 algorithms in first sector

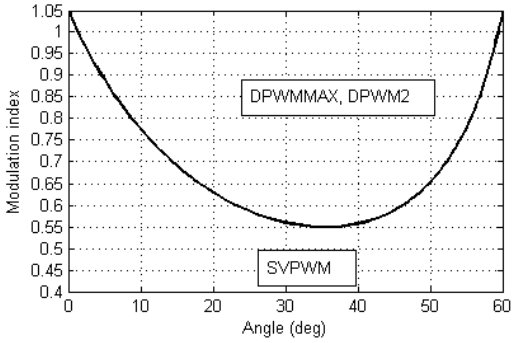

Fig. 17 boundary between SVPWM and DPWMMAX and DPWM2 algorithms in first sector

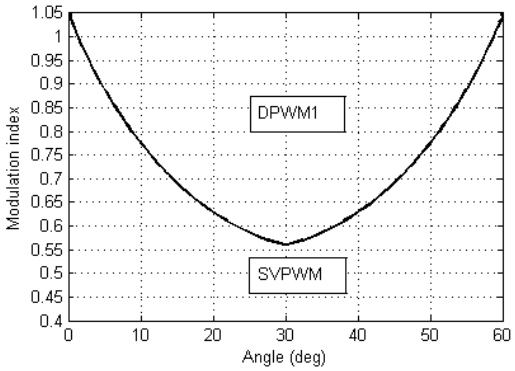

Fig. 18 boundary between SVPWM and DPWM1 algorithms in first sector

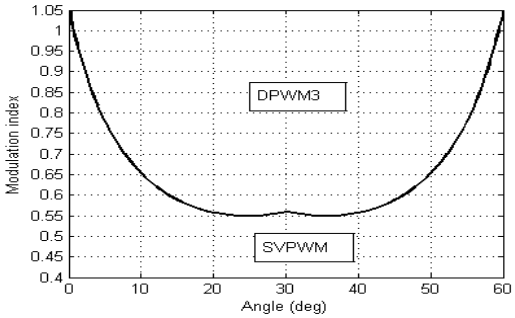

Fig. 19 boundary between SVPWM and DPWM3 algorithms in first sector

From Fig. 11 to Fig. 19, it can be observed that the SVPWM algorithm gives less harmonic distortion at lower modulation indices whereas the DPWM algorithms give less harmonic distortion at higher modulation indices. Moreover, it can be observed that at all modulation indices DPWM3 results in reduced harmonic distortion when compared with the other DPWM algorithms.

4. High Performance PWM Algorithm:

The performance analysis conducted so far clearly shows that selecting SVPWM algorithm in the lower end of the linear modulation range and DPWM3 in the remainder results in a superior overall performance when compared to the SVPWM algorithm. The proposed high-performance PWM algorithm compares the rms current ripple values of SVPWM and DPWM3 in each sampling time period and uses any one of the PWM algorithms that results in reduced harmonic distortion. The flowchart of proposed high-performance PWM (HPPWM) algorithm is shown in Fig. 20.

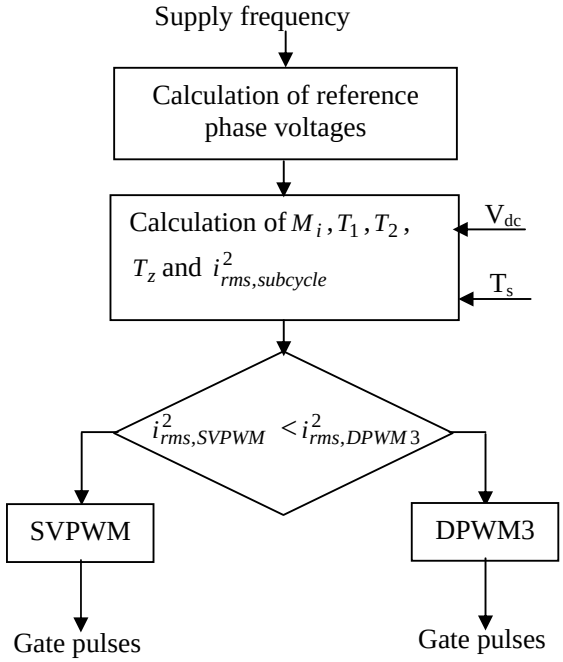

Fig. 20 flowchart of the proposed HPPWM algorithm

5. Simulation Results and Discussion:

To verify the proposed high-performance PWM algorithm, numerical simulation studies have been carried out and results have been presented. Simulation studies have been carried out at different supply frequencies (different modulation indices). The steady state current waveforms along with the total harmonic distortion (THD) values for SVPWM algorithm based drive are shown from Fig. 21 to Fig. 22. The simulation results of proposed high-performance PWM algorithm based drive are shown from Fig. 23 to Fig. 24.

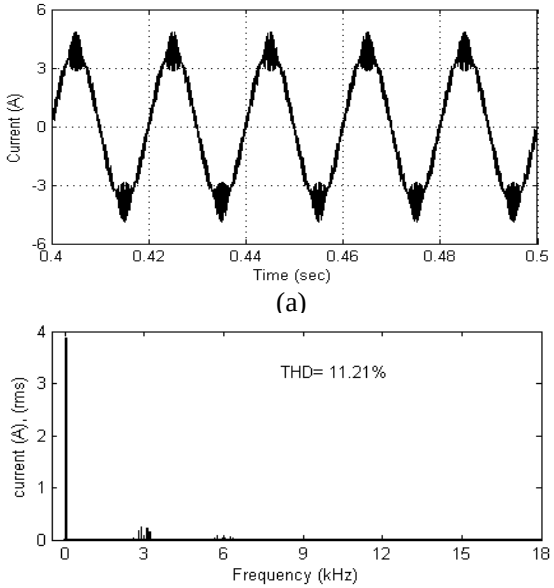

Fig. 21 simulation results of SVPWM based drive (f=50 Hz or M_i = 0.906) (a) current (b) Harmonic spectra of current

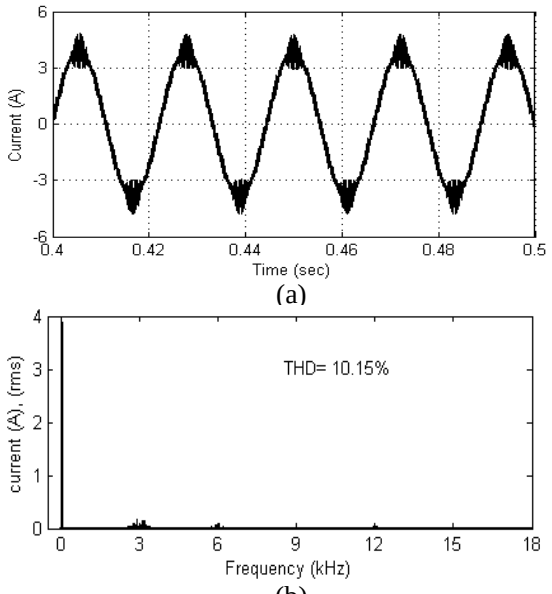

Fig. 22 simulation results of SVPWM based drive at (f=45 Hz or M_i = 0.81 (a) current (b) Harmonic spectra of current

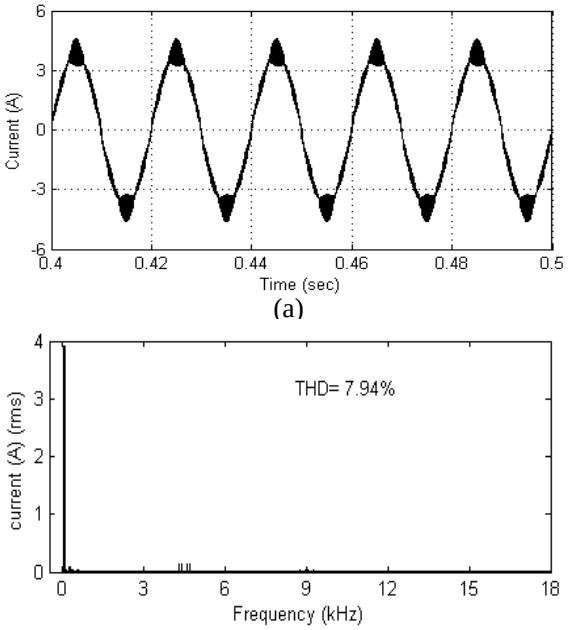

Fig. 23 simulation results of proposed high-performance PWM based drive (a) current (f=50 Hz or M_i = 0.906) (b) Harmonic spectra of current

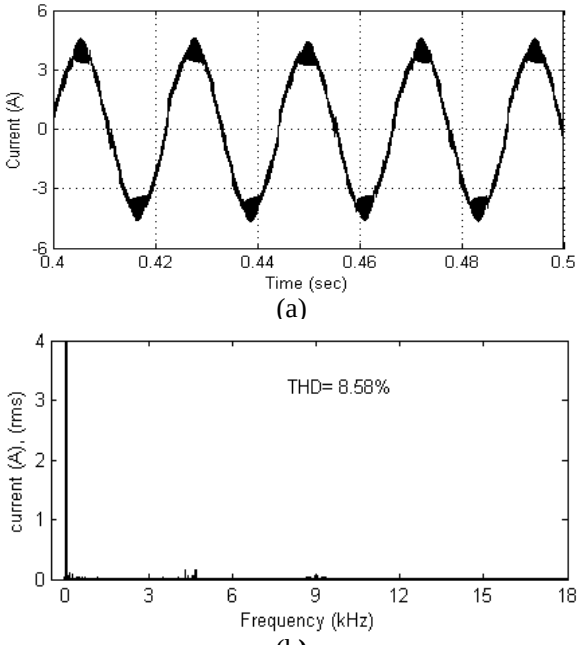

Fig. 24 simulation results of proposed high-performance PWM based drive (a) current (f=45 Hz or M_i = 0.81) (b) Harmonic spectra of current

From the simulation results, it can be observed that the proposed high-performance PWM algorithm gives superior waveform quality when compared with the SVPWM algorithm. Also, proposed PWM algorithm gives spread spectra and hence reduces the acoustical noise of the induction motor. Thus, the proposed algorithm reduces both the harmonic distortion and acoustical noise.

6. Conclusions

As the conventional space vector approach requires the angle and sector information to calculate the actual gating times of the inverter, the complexity involved in the PWM algorithm is more. To reduce the complexity involved in the conventional space vector approach, this paper presents a novel approach using the concept of offset time. By varying a constant in the generalized offset time expression, various DPWM algorithms have been developed along with the SVPWM algorithm. The harmonic analysis of the various PWM algorithms has been carried out by using the concept of current ripple. To reduce the harmonic distortion at all modulation indices, a simple high-performance PWM algorithm has been proposed by utilizing the current ripple characteristics. From the simulation results, it can be observed that the proposed high-performance PWM algorithm gives superior performance when compared with the SVPWM algorithm.

References

1. Joachim Holtz,: *Pulsewidth Modulation – A Survey*. In: IEEE Trans. Industrial Electronics, vol. 39, No.5, Dec, 1992, pp. 410-420.
2. Heinz Willi Van Der Broeck, Hans-Christoph Skudelny and Georg Viktor Stanke,: *Analysis and realization of a Pulsewidth Modulator based on Voltage Space Vectors*, In. IEEE Trans. Industrial Applications., vol. 24, No.1, Jan/Feb 1988, pp.142-150.
3. Ahmet M. Hava, Russel J. Kerkman and Thomas A. Lipo,: *A high-performance generalized discontinuous PWM algorithm*, In: IEEE Trans. Industrial Applications, vol. 34, no. 5, Sept/Oct, 1998, pp. 1059-1071.
4. Ahmet M. Hava, Russel J. Krkman and Thomas A. Lipo,: *Simple analytical and graphical methods for carrier-based PWM-VSI drives*, In: IEEE Trans. Power Electronics, vol. 14, no. 1, Jan 1999, pp. 49-61.
5. V. Blasko,: *Analysis of a hybrid PWM based on modified space-vector and triangle-comparison method*,: In: IEEE Trans. Industrial Applications, vol. 33, May/Jun, 1997, pp. 756–764.
6. Olorunfemi Ojo,: *The generalized discontinuous PWM scheme for three-phase voltage source inverters*, In: IEEE Trans. Industrial Electronics, vol. 51, no. 6, Dec, 2004, pp. 1280-1289.
7. D. Casadei, G. Serra, A. Tani, and L. Zarri,: *theoretical and experimental analysis for the RMS current ripple Minimization in induction motor drives controlled by SVM technique*, In: IEEE Trans. Industrial Electronics, vol.51, no.5, Oct, 2004, pp.1056,-1065.
8. Kaushik Basu, J. S. Siva Prasad, and G. Narayanan,: *Minimization of torque ripple in PWM AC drives*, In: IEEE Trans. Industrial Electronics, vol.56, no.2, Feb, 2009, pp.553-558.
9. Dae-Woong Chung, Joohn-Sheok Kim, Seung-Ki Sul,: *Unified Voltage Modulation Technique .for Real-Time Three-Phase Power Conversion*, In: IEEE Trans. Industrial Applications, vol. 34, no.2, March/April, 1998, pp 374-380.
10. T. Brahmananda Reddy, J. Amarnath and D. Subbarayudu, "*Improvement of DTC performance by using hybrid space vector Pulsewidth modulation algorithm*" International Review of Electrical Engineering, Vol.4, no.2, Jul/Aug, 2007, pp. 593-600.